Optical system of aplanatic telescope with a 100 m spherical primary mirror

Vladislav V. Druzhin,[a,*] **Daniil T. Puryaev**,[a] **and Alexander V. Goncharov**[b]

[a]Bauman Moscow State Technical University (BMSTU), Department of "Laser and Optoelectronic Systems" (RL-2), Moscow, Russia

[b]National University of Ireland Galway, School of Physics, NUI Galway, Galway, Ireland

Abstract. We propose an optical system of an extremely large telescope for ground-based or planetary use. The system comprises a segmented spherical mirror with a diameter of 100 m and f-number of $f/1$. There are three annular zones on the primary mirror, which corresponds to three annular telescopes (ATs) with f-numbers $f/2$, $f/3.2$, and $f/5.2$, all using a concave cardioidal secondary mirror with a maximum diameter of 3.18 m. This two-mirror system satisfies Fermat's principle and the Abbe's sine condition. The central zone of the primary mirror with a diameter of 23.8 m is used for the central three-mirror telescope, which is based on an afocal two-mirror system with a convex aspheric secondary mirror with a diameter of 3 m. Four possible configurations are presented for the central telescope, which makes it possible to vary the f-number in a wide range with design examples given for $f/1$, $f/4.2$, $f/14$, and $f/33$ systems. The ATs form three coherent images of the same astronomical object, which offers possibilities of simultaneous observations at three different wavelengths or image processing of a combined image with enhanced angular resolution. The main goal of the paper is to investigate the properties of new optical systems for ground-based and space telescopes with a fast spherical primary mirror for which aberration correction is achieved with a minimum number of auxiliary aspheric mirrors near the prime focus. [DOI: 10.1117/1.JATIS.8.2.024005]

Keywords: ground-based telescopes; telescopes; mirror system design; large observatories; aspherics; mirrors.

Paper 22007G received Jan. 18, 2022; accepted for publication Jun. 17, 2022; published online Jun. 30, 2022.

1 Introduction

Progress in our scientific exploration of the cosmos and our understanding of the Universe is directly linked with the construction and implementation of technologically more advanced optical telescopes on the ground and in space with increased aperture and sensitivity. Currently, the ground-based extremely large telescope (ELT) is under construction by the European southern observatory (ESO), which is based on a three-mirror anastigmat optical system.[1] Its nearly paraboloidal primary mirror is segmented with an overall diameter of 38.54 m and focal ratio of $f/0.89$. The diameters of the convex hyperboloidal secondary and concave aspheric tertiary mirrors are 4.2 and 3.8 m, respectively. The focal length of the telescope is 684 m. The thirty meter telescope (TMT)[2] featuring the Ritchey–Chrétien optical design with a 30-m $f/1.0$ hyperboloidal segmented primary mirror is proposed. Its primary mirror segments are in production. The main reason for primary mirror segmentation is the limits on manufacturing capabilities for large aspherical mirrors. The diameter of its convex secondary mirror is 3.1 m, and the telescope focal length is 450 m. In earlier proposals for the new generation of astronomical telescopes including the Euro50,[3] a European 50-m optical telescope based on aplanatic Gregorian design, and the Overwhelmingly Large Telescope (OWL)[4] with a 100-m spherical primary mirror, the primary mirrors were considered to be segmented. In the OWL design, a 25-m flat secondary

*Address all correspondence to Vladislav V. Druzhin, vlad.druzhin@gmail.com

2329-4124/2022/$28.00

mirror was also segmented followed by a four-mirror corrector that contained two 8-m aspheric mirrors and two smaller mirrors with diameters of 4.2 m and 2.3 m. The main drawback of the system was that the final telescope focus was located in the middle of the system near the center of curvature of the primary mirror without any provision of the Nasmyth platforms for gravity-stable operation of science instruments. The majority of the world's largest 8-m and 10-m astronomical telescopes are based on Cassegrain or Ritchey–Chrétien designs using monolithic or segmented primary mirrors. However, future telescopes with a primary mirror diameter >10 m are considered segmented only. For example, the primary mirror for the TMT features 496 hexagonal segments, each about 1.44 m across corners, whereas ELT will use 798 segments that are 1.45-m size. Due to the aspheric shape of the primary mirror, its segments will have different shape types depending on the distance of the segments to the center of the primary and the orientation of their hexagonal cut, so one has to manufacture 82 different segment types for the TMT and 133 different types for the ELT. On the other hand, for the OWL project, it was planned that the primary mirror would have 3048 identical spherical segments that are cut in the shape of 1.6-m hexagons. The main premise of the OWL design was that manufacturing of spherical segments and their subsequent cophasing would greatly simplify the task of creating a giant 100-m primary mirror.

The primary mirrors of space telescopes also have large diameters, and the mirrors have to be produced as segmented structures with many fragments. In addition to aspherical mirror manufacturing limitations, the segmentation of the main mirrors of space telescopes is associated with the size of the launch vehicle, currently not exceeding the size of 5 m, and they require a complex deployment scheme. The adaptation of the telescope in space has many problems and requires the application of complicated solutions and special techniques. The primary mirror of James Webb Space's Telescope[5] consists of 18 hexagonal mirror segments measuring 1.32 m in diameter, which are combined to create a 6.5-m diameter concave parabolic mirror. The Millimetron space observatory (Spektr-M)[6] is based on the Cassegrain telescope system with the main parabolic mirror having a diameter of 10 m and a focal length of 2400 mm. The main parabolic mirror is a segmented form with 96 parabolic submirrors with various configurations of four standard sizes. After the telescope is placed on the orbit, the telescope must be positioned or adapted. Several concepts of the Origin[7,8] telescope project consider segmentation of the 5.9-m-diameter elliptical primary on 37 hexagonal segments, each 1.277-m, or on 18 segments of two different prescriptions arranged in two annuli (six inner segments with a radial width of 1.2 m and 12 outer segments with a radial width 1.294 m) that together form a circular 5.9-m aperture. In comparison with telescopes with an aspheric primary, having spherical symmetry and accessible common center of curvature for all segments is a great advantage for their alignment. In this regard, the spherical primary mirror offers many advantages for optical telescopes with apertures >50 m. The main goal of the paper is to present the results of finding new optical systems for ground-based and space telescopes in which the correction of spherical aberration of the primary mirror is achieved with a minimum number of additional aspheric mirrors near its prime focus.

2 Telescope Optical System

The proposed system shown in Fig. 1 is essentially two coaxial telescopes using a common 100-m $F/1$ primary spherical mirror. The entrance pupil is defined by the edge of the primary mirror of the telescope and consists of three annular zones and one central zone as shown in Fig. 2.

The diameter of the individual annular zones in the pupil is given in Table 1. The light-collecting area of the telescope with a pupil diameter of 100 m is 7854m^2, and the area of the first zone is 61.3% of the total area, 23.8% for the second zone, 9.2% for the third zone, and 5.7% for the central zone.

The optical system uses two configurations with a segmented concave secondary mirror M_2 for the first three annular zones and a monolithic convex secondary mirror M_3 for the central telescope.

The reflecting surface of M_2 is formed by axial revolution of a cardioid curve (in a particular case, it is known as Pascal's snail) around the optical axis. The focusing system containing the

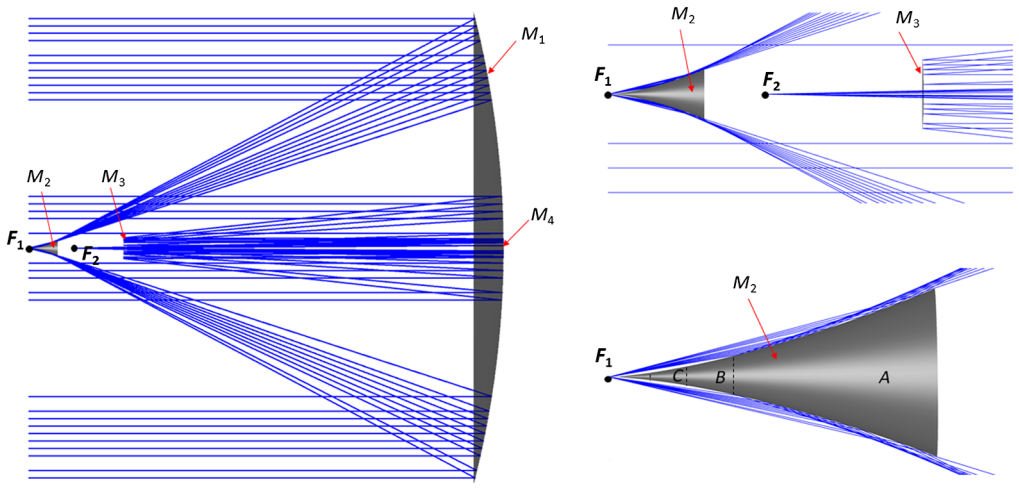

Fig. 1 Baseline telescope layout: M_1 is the spherical primary mirror, M_2 is the segmented concave secondary mirror (A, B, C are the annular segments), M_3 is the convex monolithic secondary mirror of the afocal telescope, and M_4 is the focusing mirror of the central telescope.

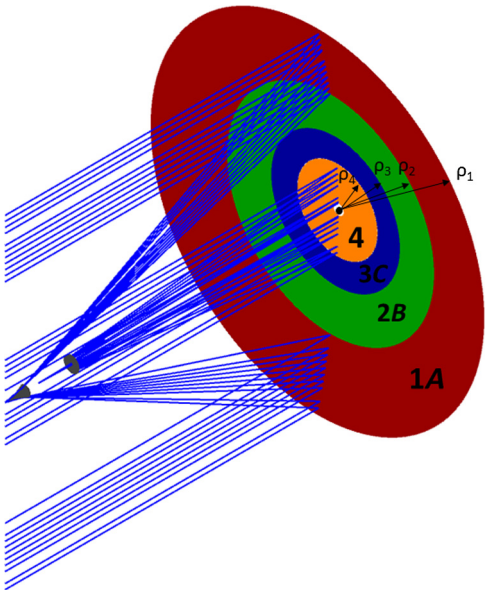

Fig. 2 Entrance pupil of the telescope: 1, 2, and 3 are the annular zones in the pupil with the corresponding sections A, B, and C on the secondary mirror; these zones have different arrangements for image formation. Zone 4 is the central zone.

Table 1 Parameters of the entrance pupil.

Entrance pupil zone radius	Value, m
ρ_1	50.00
ρ_2	31.10
ρ_3	19.27
ρ_4	11.92

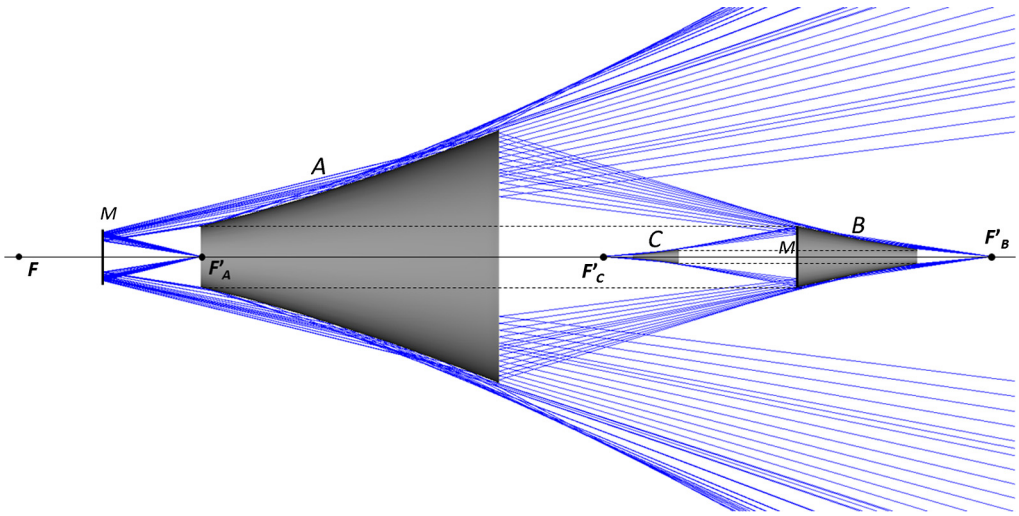

Fig. 3 Three different arrangements for reflections from sections *A*, *B*, and *C* of secondary mirror M_2.

first (outer) annular zone and two inner zones of the spherical primary mirror M_1 and the cardioidal mirror M_2 is a two-mirror aplanatic telescope with the focal length equal to the radius of curvature of the primary mirror, which is chosen to be 200 m. We call this telescope an annular telescope (AT) due to its annular shape of the entrance pupil with the inner radius of 11.92 m. The main optical property of the AT is that it is an aplanatic system. It provides perfect imaging of an axial point for which Fermat's principle and the Abbe sine condition are fulfilled. The profile of the secondary mirror M_2 is given by the cardioid curve, which is uniquely defined by the radius of curvature of the primary mirror M_1, because the cardioid curve extends exactly to the paraxial focus of M_1. Due to the fact that some rays reflected from the inner zones of M_1 can be obscured by the outer edge of the secondary mirror M_2, we consider three annular sections A, B, and C on M_2 and thus avoid the ray obscuration problem using plain mirrors as indicated by dashed vertical lines in Fig. 1. A detailed view of three different ray paths with reflection from annular segments A, B, and C of M_2 are shown in Fig. 3. The plain mirrors positioned perpendicular to the optical axis are marked by M in Fig. 3.

Figure 2 shows $1A$, $2B$, and $3C$ zones, where $1A$ means that the rays passing through the first (outer) zone on M_1 reflect from section A on M_2 and form an image at focus F; similarly $2B$ zone means that the rays passing through the second annular zone on M_1 are redirected by a plain mirror M toward section B of M_2 and, after reflection from it, form an image at focus F'_B. Finally, $3C$ means that the rays passing through the third innermost annular zone on M_1, and reflecting from two plain mirrors reach section C and, after reflection, form an image at focus F'_C. An afocal two-mirror system with M_1 and M_3 together with a focusing mirror M_4 constitute the central telescope system. Having access to several focii makes this telescope a bifocal telescope.

3 Optical System of the Annular Telescope (AT)

The main element of the AT is the secondary mirror M_2 with the surface formed by revolution of the cardioid curve around the symmetry axis. This mirror is placed at the paraxial focus of the spherical primary mirror. The two mirrors form an aplanatic system (both Fermat's principle and the Abbe sine condition are fulfilled). The meridional profile of the secondary mirror is expressed in a parametric form for the height $y(\phi)$ and the sag $z(\phi)$

$$y = R\,\sin(\phi)(1-\cos(\phi)), z = R\,\cos(\phi)(1-\cos(\phi)), \tag{1}$$

where R is the radius of curvature of the spherical primary mirror, ϕ is the incidence angle between the incoming ray and the normal to the spherical surface at the incident point, $d = R/2$ is the axial distance between the mirrors, and O is the origin of the Cartesian coordinate system

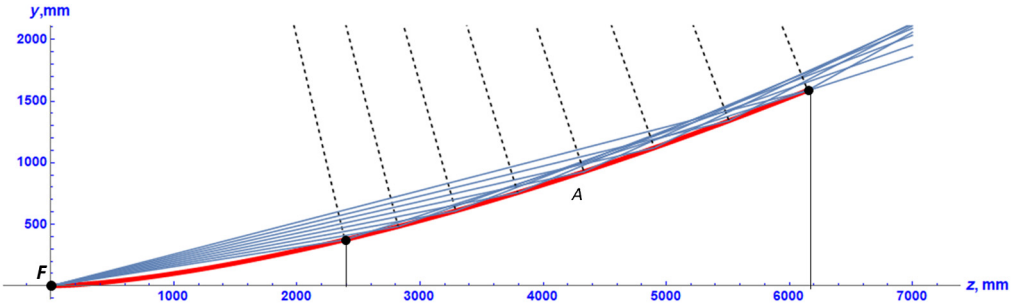

Fig. 4 Secondary mirror profile with ray-tracing for annular zone 1 and section *A*.

y, z, which is placed at the vertex of the secondary mirror in the paraxial focus of the primary. The ray after reflection from the secondary mirror is redirected toward the paraxial focus of the primary (Fig. 4) such that the angle between the ray and the optical axis is ϕ.

Using well-known coordinate transformations for Eq. (1), we describe the profile of the secondary mirror in polar coordinates as

$$\rho = R(1 - \cos(\phi)), \tag{2}$$

where ϕ is the angle between the ray and the normal to the spherical surface at the incident point and ρ is the radial coordinate, which is the distance from the incident point to the symmetry axis. In the Cartesian coordinate system, the mirror profile is given in an implicit form $F(x, y, z) = 0$:

$$-R^2y^2 + 2R(z(y^2 + z^2)) + (y^2 + z^2)^2 = 0. \tag{3}$$

Solving Eq. (3) for y, we find the secondary mirror profile as an explicit function $y = f(z)$:

$$y = \sqrt{\frac{1}{2}(R^2 - \sqrt{R^3(R - 4z)} - 2Rz - 2z^2)}. \tag{4}$$

Alternatively, if one needs to determine the surface sag z as a function of the transverse coordinate y, the following expressions is used:

$$\begin{aligned}
z &= \frac{\sqrt{a_1}}{2} - \frac{\sqrt{a_2}}{2} - \frac{R}{2}, \\
a_1 &= \frac{2R^3}{\sqrt{a_2}} - a_3 + 2R^2 - \frac{8y^2}{3}, \\
a_2 &= a_3 + R^2 - (4y^2)/3, \\
a_3 &= \frac{4\,2^{2/3}a_4}{3\sqrt[3]{a_5}} + \frac{1}{3}\sqrt[3]{2a_5}, \\
a_4 &= 3\sqrt[3]{a_3} + \frac{1}{3}\sqrt[3]{2a_5}, \\
a_5 &= -27R^4y^2 + 72R^2y^4 + 3\sqrt{81R^8y^4 - 48R^6y^6} - 32y^6.
\end{aligned} \tag{5}$$

Table 2 presents the geometrical and photometric properties for each annular zone in the entrance pupil of the AT. The table lists the numerical aperture defined as $\sin(\phi)$ and the transmission coefficient τ calculated based on the area of the annular zone; therefore, the product $\tau \sin^2(\phi)$ is the realistic light-gathering power taking into account that only a fraction of the total light enters one annular zone. The first trajectory of rays passing through the first pupil zone that gathers most of light is taken as a reference of light-gathering power for other zones and is characterized by the coefficient K listed in Table 2. Three different trajectories of rays form three coherent images at focii F'_A, F'_B, and F'_C. This aspect can be regarded as a drawback, but it

Table 2 Comparison of physical apertures.

Ray trajectory	$\sin(\phi)$	τ	$\tau \sin^2(\phi)$	K
1	0.25	0.613	0.0383	1
2	0.156	0.238	0.00576	0.151
3	0.096	0.092	0.000851	0.022

can be also beneficial if one requires imaging of the same scientific target at three different spectral bands simultaneously. These three focii provide the coherent image of the same object and can be combined into one when imaging in the same spectral band. This is the reason that we refer to this telescope as a bifocal system. Also, the trajectory of the third zone can be used, for example, for cophasing of the second and first zone if the spherical segments overlap at the border with the first and the third annular zones, so one can align all three zones using the second zone as a common part for the neighbor zones. The focal length of the AT is 200 m.

4 Optical Scheme of an Afocal Two-Mirror System (ATS)

The afocal two-mirror Mersenne system is well known in astronomical optics. The system consists of two paraboloidal mirrors with their focii being coincident with one another. An afocal two-mirror system (ATS) with corrected spherical aberration is considered to be an ideal system because paraboloidal mirrors are free from spherical aberration for any aperture size. The Mersenne system discovered in 1648, remained the only known ideal ATS. A new afocal two-mirror system was proposed in 1988 with an infinite number of possible solutions for an ideal ATS.[9,10] These solutions for an ideal ATS are based on Fermat's principle. Figure 5 shows an ATS that consists of the concave primary OM and convex secondary oB mirrors with their surface shapes being interrelated but not explicitly defined in advance. We use two coordinate systems, namely zoy for the secondary mirror oB and ZOY for the primary mirror OM.

The horizontal axes oz and OZ coincide with the optical axis of the system. According to Fermat's principle, the optical path for a ray at the height Y from the optical axis is equal to the optical path of a paraxial ray, i.e., $ABMN = 2d$, where d is the axial distance between the

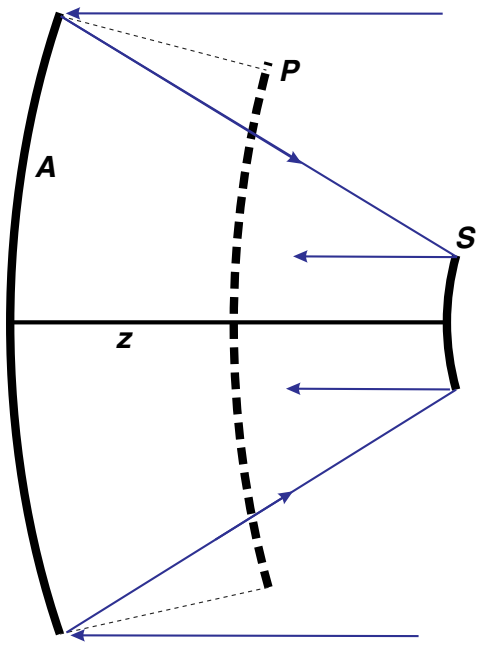

Fig. 5 Optical layout of an afocal two-mirror system (ATS).

mirrors. The surface normals at the reflection points B and M make the same angles with respect to the optical axis; this angle is φ. Using geometric properties of reflecting surfaces, from Fig. 5 we find the following relations:

$$Y - y = 2d\ \tan(\varphi), \quad Z - z = d\tan^2(\varphi). \tag{6}$$

If the secondary mirror oB has a spherical shape with a radius of curvature r, then the meridional profile of the primary mirror OM is found in the parametric form, where the angle φ of the normal is used as a parameter:

$$Y = r\ \sin(\varphi) + 2d\ \tan(\varphi), \quad Z = r(1 - \cos(\varphi)) + d\tan^2(\varphi). \tag{7}$$

From paraxial optics, it follows that for an afocal system $R = r + 2d$, where R is the radius of curvature at the vertex of the primary mirror OM. Figure 5 shows point E, which is the paraxial center of curvature of the mirror OM, whereas MT and BC are the surface normals at points M and B for the incoming and outgoing rays, respectively. The segment ET $= \Delta S_n$ is the longitudinal aberration of the surface normal. From the expression above it follows that $\Delta S_n = d\ \tan(2\varphi)$. It is worth noting that the aberration of a normal to the surface of a parabolic mirror with the focal length $f = d$ has exactly the same expression. This observation brings us to an important property of the aspheric mirror A shown in Fig. 6: its surface is equidistant from a virtual paraboloidal mirror P with the focal length $f = d$ and its vertex being axially shifted from A by the distance equal to the radius of curvature r of the spherical mirror S. If we consider the surface of the aspherical mirror A [see Fig. 6(a)] as a wavefront traveling in a homogeneous medium toward its center of curvature, then at a distance r (being the radius of curvature of mirror S), it will assume a shape of a paraboloid of revolution P (a virtual paraboloidal mirror). Due to this remarkable property, we call this aspheric mirror A an equi-paraboloidal mirror.

From analytical geometry it follows that the meridional profiles of mirror A and virtual paraboloid P have a common evolute.

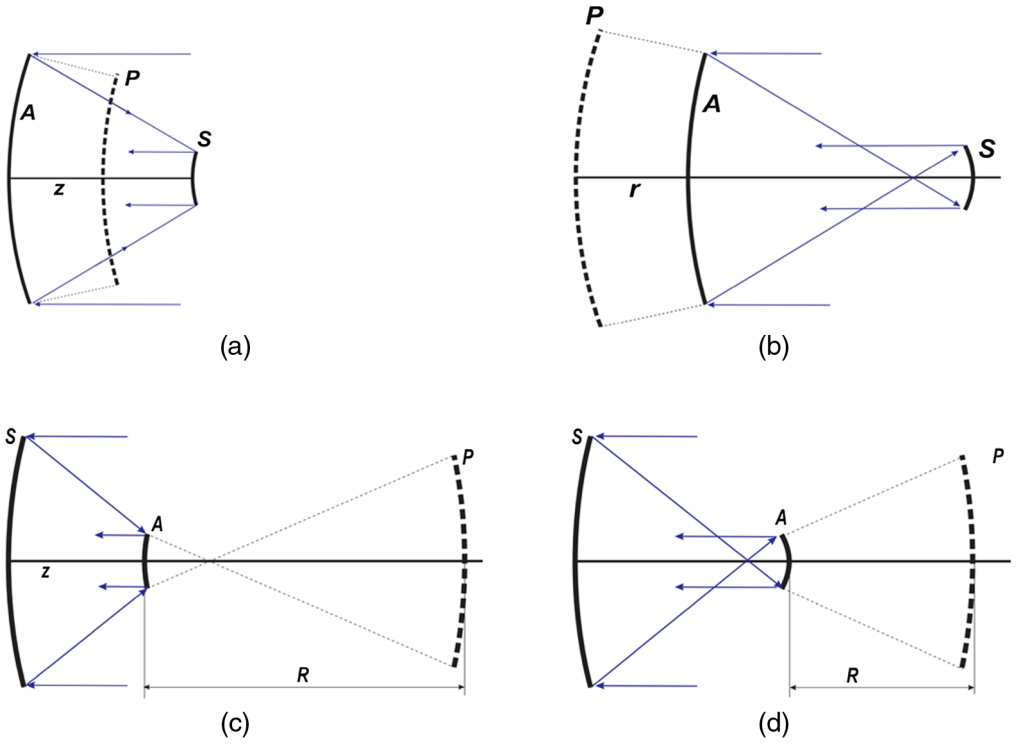

Fig. 6 Two-mirror afocal systems (a), (b), (c), and (d) with spherical mirror S and equi-paraboloidal mirror A for virtual paraboloidal mirror P.

If the primary mirror (OM in Fig. 5) is spherical with the radius of curvature R, then the meridional profile of the secondary mirror is defined by the parametric equations

$$y = R\,\sin(\varphi) - 2d\,\tan(\varphi), \quad z = R(1-\cos(\varphi)) - d\tan^2(\varphi). \tag{8}$$

The structures of Eqs. (7) and (8) are nearly identical with the only difference being due to the opposite sign for the axial distance d. Four possible combinations for the two-mirror afocal system with one spherical mirror S and the other equi-paraboloidal mirror A are shown in (a)–(d) of 6, where the position of the virtual paraboloidal mirror P is also indicated. Knowing the position of the virtual mirror P, one can choose an optimal scheme for optical testing of the aspheric mirror A by means of an optical corrector (nulling lens) that is used for testing paraboloidal mirrors.

Similar to the case of the two-mirror Mersenne system the proposed ideal afocal system is free from spherical aberration regardless of the aperture size or system magnification. For any given shape of one mirror, the shape of the other mirror is well defined in a parametric form. To summarize the properties of the ideal afocal system, we formulate the following two theorems:

1. For any given shape of one of the mirrors in the system, the shape of the other mirror is uniquely defined. Therefore, there exists an infinite number of ideal afocal systems for which the mirror shapes are interrelated according to Eq. (6), where d is the axial distance between the mirrors and φ is the angle between the normal to the surface at the point of incidence and the optical axis.
2. If one of the mirrors has a spherical shape, then the other mirror becomes an equi-paraboloidal mirror, that is, its surface is equidistant from a virtual paraboloidal mirror with the focal length equal to the axial distance d.

In the case of the primary mirror having a spherical shape and the secondary mirror being convex, as shown in Fig. 6(c), aspheric meridional profile of the secondary mirror is given as

$$y = R\,\sin(\varphi) - 2d\,\tan(\varphi), \quad z = R(1-\cos(\varphi)) - d\tan^2(\varphi). \tag{9}$$

In the case of a negative sign of y in Eq. (9), the shape of secondary mirror becomes concave, as shown in Fig. 6(d).

5 Design Examples for the Afocal Two-Mirror Central Telescope

The central zone of the primary mirror with a diameter of 23.8 m and the convex aspheric secondary mirror M_3 (shown in Fig. 7) with a diameter of 3-m constitutes an afocal two-mirror system that forms a collimated beam propagating toward the primary spherical mirror.

After reflection from the primary mirror, an image of a star is formed in the paraxial focus of the spherical mirror, as shown in Fig. 8(a), and the secondary mirror M_3 needs a central opening to allow the focused beam to pass through. It is easy to show that the axial beam, after second reflection from the spherical mirror, will travel back to the secondary mirror M_3, and the beam diameter on M_3 will be 0.382 m. In this central region, one could place a flat mirror or a concave hyperboloidal mirror in front of M_3, so the focal length of the central telescope can be changed within a broad range.

As a concrete example, we use a 0.382-m hyperboloidal mirror with the radius of curvature of $R_0 = 4.74503$ m and conic constant $k = -1.88379$. For this configuration, the focal length of

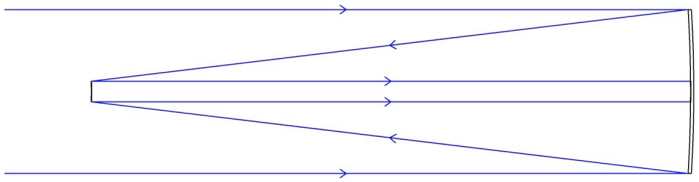

Fig. 7 Afocal two-mirror system of the central telescope.

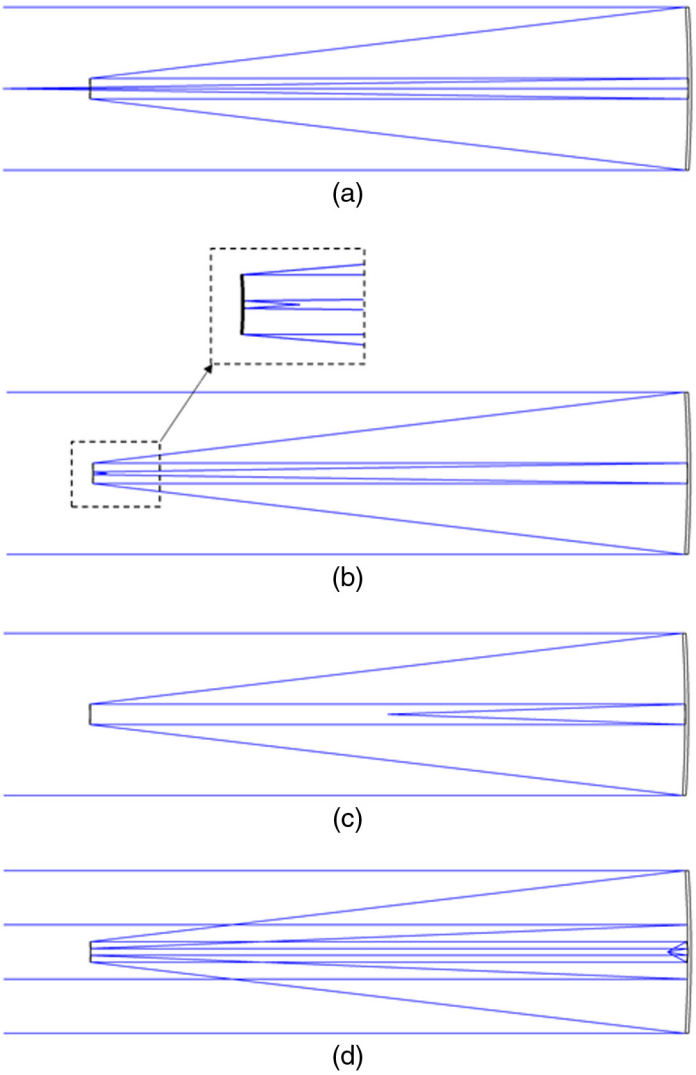

Fig. 8 Combination of ATS of the central telescope with different focusing mirrors: (a) with the primary spherical mirror; (b) with a hyperbolic mirror; (c) with a spherical mirror (Schmidt type system) for which $R = 87.262$ m; and (d) with a parabolic mirror.

the central telescope becomes 123.263 m and the offense against the sine condition is only 1.48%. If we use a 0.382-m hyperboloidal mirror with the radius of curvature of $R_0 = 3.7187$ m and conic constant $k = -1.66912$, then the focal length can be reduced to 100 m, which is equal to the focal length of the primary spherical mirror; see Fig. 8(b). In this case, offense against the sine condition is 1.604%, which is still acceptable. If we use a flat mirror, rather than a hyperbolodial mirror, or simply let the axial beam pass through the central opening in M_3, then the focal length of the central telescope is equal to the product of the primary mirror focal length and the angular magnification of the two-mirror afocal system $f_{M1} \times \beta = 100$ m $\times 7.85 = 785$ m. In this case, offense against the sine condition is 1.24%; see Fig. 8(a).

An alternative system of the central telescope shown in Fig. 8(c) is based on the principle of a Schmidt system. The idea is to use a spherical mirror positioned at the vertex of the primary mirror, with the radius of curvature being equal to the axial distance $d = R = 87.262$ m between the primary and secondary mirror in the two-mirror afocal system. In this case, the center of curvature of the spherical mirror (its diameter is 3 m, the same as for the secondary mirror M_2) coincides with the vertex of the secondary mirror. The secondary mirror plays a role in the aperture stop. This configuration allows one to increase the field of view because it works as a Schmidt system.

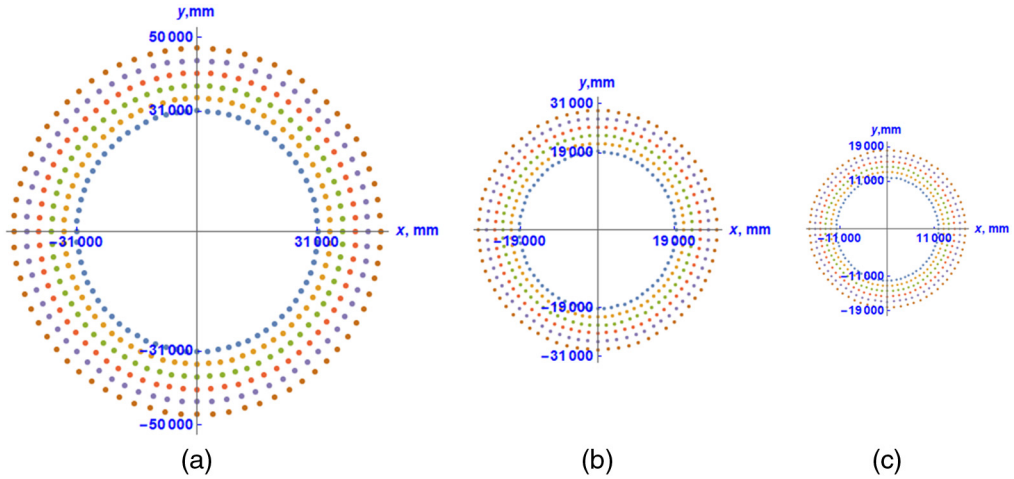

Fig. 9 Ray pattern selection of the annular zones 1 (a), 2 (b), and 3 (c) for spot diagrams calculation. Each annular zone was divided into six rings with 72 points on each ring, totally 432 beams being used for each annular zone.

The last example (d) is an afocal two-mirror system combined with a paraboloidal mirror having a vertex radius of curvature of 6 m; the focal ratio of this system is 1. The common afocal two-mirror system used for all variants is shown in Fig. 9; the radius of curvature of the primary mirror $R = 200$ m, and the vertex radius of curvature of the convex secondary mirror $r_o = 25.4757$ m. The axial distance between the mirrors $d = f_1 - f_2 = 87.2622$ m. The paraxial magnification of the system $\beta_0 = 7.85062$. For the marginal ray at the height 11.921 m, its angle with the optical axis is given as $\sin(\varphi) = 0.0595$. From the simple calculation, the marginal ray height on the secondary mirror is $y = 1.5$ m; therefore, the magnification of the system at the edge zone $\beta = 11.9214/1.5 = 7.9476$. The offense against sine condition is $\frac{\Delta\beta}{\beta_0} = \frac{\beta-\beta_0}{\beta_0} = 1.235\%$.

This is acceptable value; the Abbe Sine condition is nearly fulfilled for all systems.

6 Ray-Tracing Analysis

To perform ray-tracing in the AT, we developed our own ray-tracing code in the *Mathematica*® package. Proprietary optical design programs (*OpticStudio*®, *CODEV*®, *OSLO*®, etc.) do not allow for direct application of Eq. (1) describing the aspheric surface of the secondary mirror in the parametric form (the sag z expansion into a series leads to fractional powers of y). The tracing of the axial and off-axis beams was performed based on Eqs. (4) and (5), which enable us to determine the beam propagation directions after reflection from the secondary mirror. The initial ray pattern selected individually for each subaperture is shown in Fig. 9 with the x- and y-coordinates at the entrance pupil plane.

The results of ray-tracing analysis for the AT are presented by the spot diagrams in the focal planes as shown in Fig. 10.

The wavelength λ is defined by the f-number and the Airy disk diameter D_0 as $\lambda = D_0/1.22/(f/D)$, where D_0 is assumed to be equal to the RMS spot diameter at the edge of the field ($\omega = 1$ arcsec or = 2 arcsec). The field size is chosen such that the shortest wavelengths for the AT are located in the visible part of the spectrum. To keep the full field $2\omega = 1$ arcsec the same for all three tracks in the AT, we made an exception and equated the Airy disk diameter to the geometrical spot diameter at the edge of the field.

As a working example of the AT, we consider three cases, shown in Fig. 8, when observing at three paraxial focal planes over the full field of $2\omega = 1$ arcsec. For annular zone 1, if we use the wavelength $\lambda = 0.4$ microns and the field angle $\omega = 0.5$ arcsec, the geometrical spot diameter is equal to the Airy disk diameter, which is 1.97 microns. The linear field size is $2\omega f' = 2 \times 0.485 = 0.97$ mm, so we have $0.97/0.00197 = 492.4$ Airy disks across the full

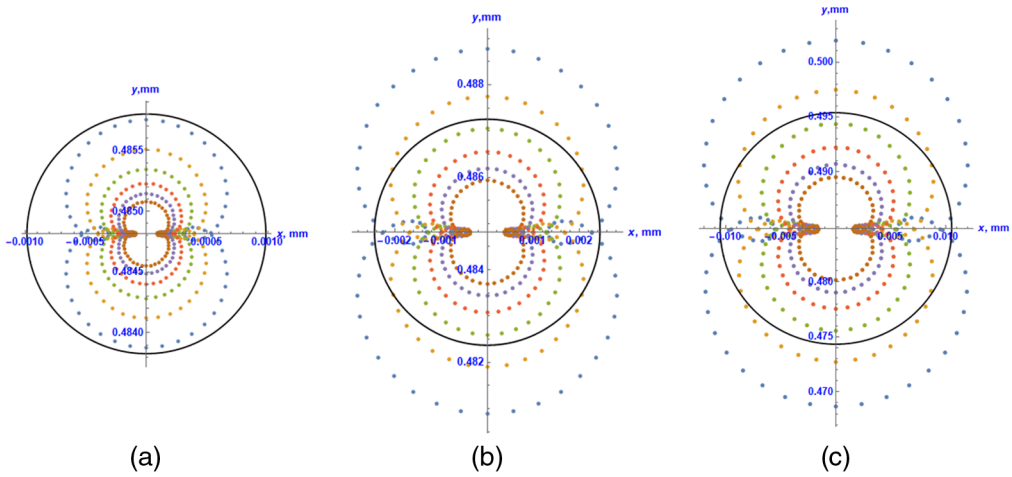

Fig. 10 Spot diagrams for off-axis field point at the edge of the field $\omega = 0.5$ arcsec for annular zone 1 at the wavelength $\lambda = 0.4$ microns (a), for zone 2 at $\lambda = 0.618$ microns (b) and for zone 3 at $\lambda = 1.028$ microns (c).

field. Using Nyquist sampling of two pixels per Airy disk radius (or 4 pixels per Airy disk), we need $4 * 492.4 = 1970$ pixels across the field with the pixel size of $1.97/4 = 0.49$ microns. Therefore, at the focal plane for zone 1, a detector with about 2000×2000 pixels (a 4-megapixel detector) is needed.

For annular zone 2, if we use the wavelength $\lambda = 0.618$ microns and the field angle $\omega = 0.5$ arcsec, the RMS spot diameter is equal to the Airy disk diameter, which is 4.87 microns. For this focal plane, we have about 200 Airy disks across the field, and a 0.64-megapixel detector could be used.

Finally for zone 3, if we use the wavelength $= 1.028$ microns and the field angle $=$ 0.5 arcsec, the RMS spot diameter is 21.06 microns, and for this focal plane, we have 46 Airy disks across the field, which corresponds to about 200×200 pixels

Finally, for zone 3, if we use the wavelength $\lambda = 1.028$ microns and the field angle $\omega = 0.5$ arcsec, the RMS spot diameter is equal to the Airy disk diameter, which is 21.06 microns. For this focal plane, we have $0.97/0.02106 = 46$ Airy disks across the field and a detector with about 200×200 pixels is required.

Due to image quality limited by astigmatism, the number of resolvable elements in the image across the field of any given zone is inversely proportional to the wavelength used and one can use the working example for scaling to another wavelength. It is clear that the AT is more suitable for observations at shorter wavelengths; however, using several focal planes makes it possible to observe the same object simultaneously at different wavelengths.

The results of ray-tracing analysis for the four variants telescope presented as the spot diagrams in the focal plane using the *OpticStudio*® SW tool are shown in Figs. 11–14. As a working example of the central telescope, we consider four different cases.

For variant 1 of the central telescope, if we use the wavelength $\lambda = 1.97$ microns and the field angle $\omega = 2$ arcsec, the RMS spot diameter is equal to the Airy disk diameter, which is 158.6 microns. The linear field size is $2 \times 7.706 = 15.412$ mm, so we have $15.412/0.1586 =$ 97.2 Airy disks across the full field. Using Nyquist sampling of four pixels per Airy disk, we need $4 \times 97.2 = 388$ pixels across the field with the pixel size of $157.1/4 = 39.65$ microns. For variant 2 of the central telescope, if we use the wavelength $\lambda = 3.20$ microns and the field angle $\omega = 2$ arcsec, the RMS spot diameter is 8.23 microns, which corresponds to about 74 Airy disks (about 300 pixels) across the field. For variant 3 of the central telescope, if we use the wavelength $\lambda = 6.78$ microns and the field angle $\omega = 2$ arcsec, the RMS spot diameter is 237.8 microns, and we have 28 Airy disks (113 pixels) across the field. Finally, for variant 4 of the central telescope, for the wavelength $\lambda = 13.7$ microns and the field angle $= 2$ arcsec, the RMS spot diameter is 33.4 microns, and we have only 15 Airy disks (60 pixels) across the field.

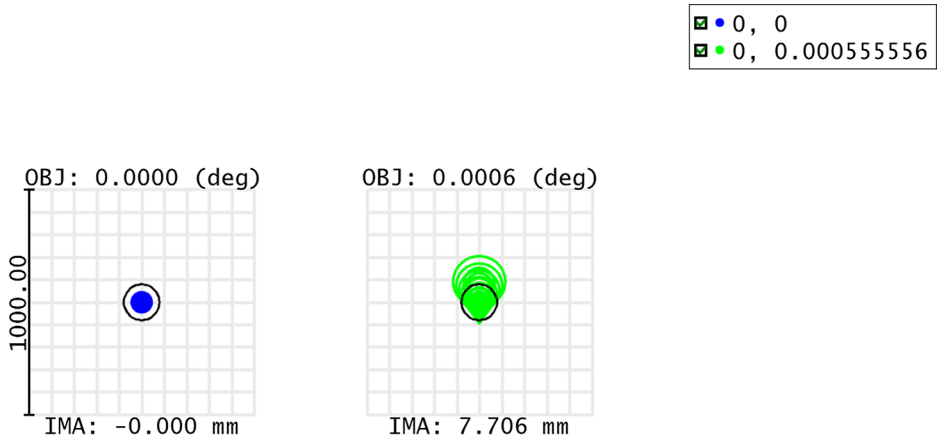

Fig. 11 Spot diagrams for the central telescope based on an afocal telescope system and concave spherical mirror with $R = 200$ m (EFFL of the telescope $= 785.062$ m, the f-number is $f/33$).

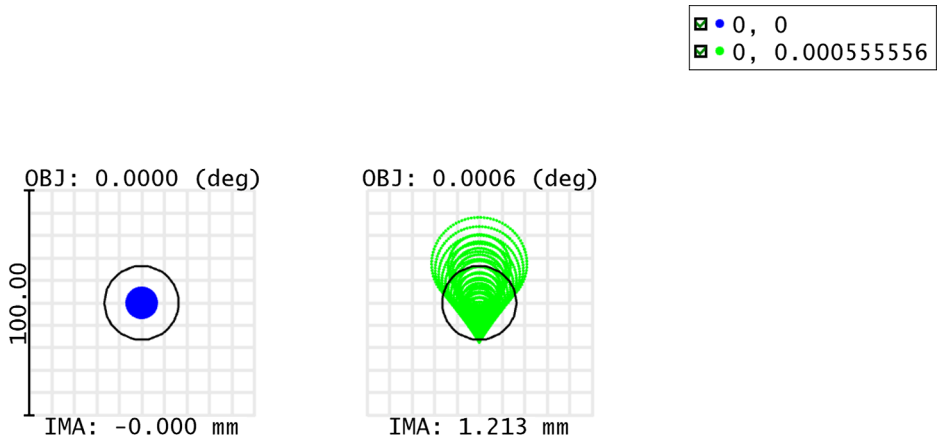

Fig. 12 Spot diagrams for central telescope based on an afocal telescope system and concave hyperbolic mirror with $R_0 = 3.7187$ and $k = -1.66912$ (EFFL of the telescope $= 100$ m, the f-number is $f/4.2$).

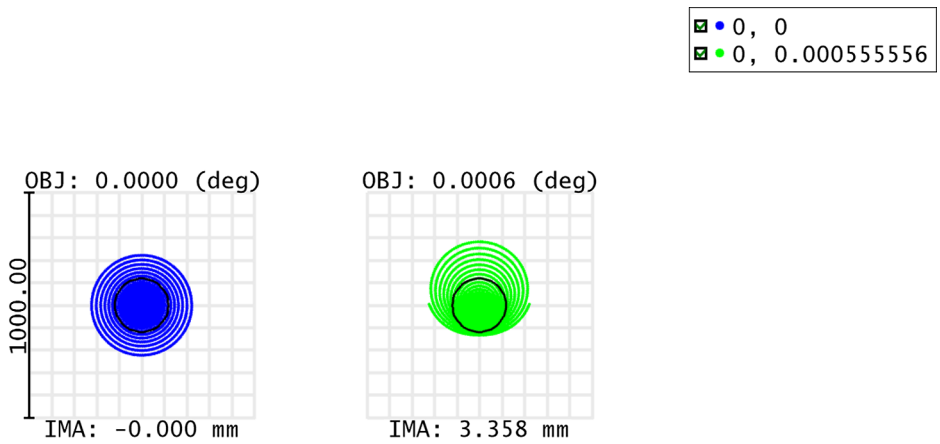

Fig. 13 Spot diagrams for central telescope based on an afocal telescope system and Schmidt system based on concave spherical mirror with $R = d = 87.2622$ m (EFFL of the telescope = 342.531 m, the f-number is $f/14.37$).

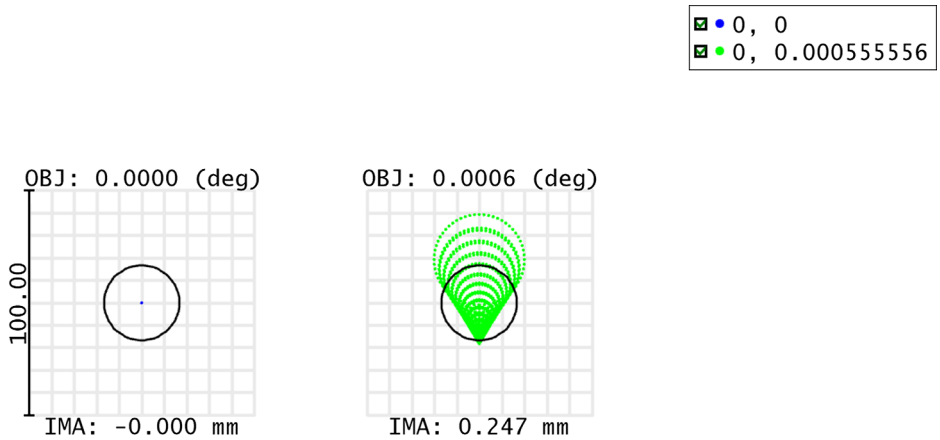

Fig. 14 Spot diagrams for central telescope based on an afocal telescope system and concave parabolic mirror with $R_0 = 6.074$ m, $k = -1$ (EFFL of the telescope = 23.842 m, the f-number is $f/1$).

Table 3 Comparison of the physical aperture ratio.

Optical system	$\sin\phi$	τ	$\tau\sin^2\phi$	K
Annular zone 1 (1:2)	0.25	0.613	0.0383	1.0
Annular zone 2 (1:3.22)	0.156	0.238	0.00576	0.151
Annular zone 3 (1:5.2)	0.096	0.092	0.000851	0.022
CT v.1 (1:33)	0.015	0.984	0.00022	0.006
CT v.2 (1:4.2)	0.1173	0.984	0.01355	0.3538
CT v.3 (1:14)	0.0344	0.984	0.0012	0.03
CT v.4 (1:1)	0.4655	0.984	0.2133	5.56

Table 4 Comparison of the spot diameters.

Optical system	ω, arcsec	D_0, μm (RMS)	ψ, arcsec
Track 1 (1:2)	0.5	1.97	$1.20\ 10^{-3}$
Track 2 (1:3.22)	0.5	4.87	$5.03\ 10^{-3}$
Track 3 (1:5.2)	0.5	21.06	$2.17\ 10^{-2}$
CT v.1 (1:33)	2	158.6	$4.17\ 10^{-2}$
CT v.2 (1:4.2)	2	32.9	$6.79\ 10^{-2}$
CT v.3 (1:14)	2	237.8	$14.32\ 10^{-2}$
CT v.4 (1:1)	2	33.4	$2.89\ 10^{-2}$

In contrast to the AT, the number of resolvable elements across the diffraction-limited field of the central telescope cannot be increased or decreased when scaling the wavelength in these four variants. This is because the field size of the central telescope is limited by coma. However, as can be seen from the working examples, the number of resolvable elements in the diffraction-limited field of the central telescope is comparable to that of the AT. The central telescope offers the possibility of observing the object at another wavelength comparable to angular resolution.

In a summary we present the results of the system evaluation based on ray-tracing and spot diagrams in Tables 3 and 4, where the following parameters are used: $\sin(\varphi)$ is the numerical aperture, τ is the transmittance of the optical system, $\tau\sin^2(\phi)$ is the physical aperture ratio, K is the coefficient of comparison of the physical aperture ratio for the selected system and the system for the first track, ω is the half-angle of the full field of view, D_{Airy} is the Airy disc diameter for a specific wavelength λ, D_0 is the RMS spot diameter in the focal plane, ψ is the angular size of RMS spot diameter $\psi = 2\arctan(\frac{D_0}{2\text{EFFL}})$, and CT is the central telescope with four configurations: $V.1 - f = 785.062$ m, $f/33$; $V.2 - f = 100$ m, $f/4.2$; $V.3 - f = 342.531$ m, $f/14$; and $V.4 - f = 23.842$ m, $f/1$.

7 Conclusion

In comparison with the known optical systems of large astronomical telescopes with an aspheric primary mirror, the proposed optical system of a telescope has functional and technological advantages in view of the spherical shape of its primary mirror. For the purpose of highlighting the differences, a comparison of all design configurations utilizing annular zone and the central telescope is summarized in Table 5. We should point out that not all configurations have an

Table 5 Summarizing table showing the telescope parameters.

Telescope	Optical system	Outer/inner, EPD, m	Secondary mirror diameter, m	EFFL, m	Wavelength, μm	Linear size of the field, mm	Number of pixels
AT	Annular zone 1	100.0/62.2	3.2	200.0	0.4	0.97	2000×2000
	Annular zone 2	62.2/38.54	0.8	200.0	0.618	0.97	800×800
	Annular zone 3	38.54/23.84	0.2	200.0	1.028	0.97	200×200
Central telescope (CT)	CT v.1	23.84/3.0	3.0	785.062	1.97	15.412	388×388
	CT v.2	23.84/3.0	3.0	100.0	3.2	2.426	295×295
	CT v.3	23.84/3.0	3.0	342.531	6.78	6.716	113×113
	CT v.4	23.84/3.0	3.0	23.842	13.7	0.494	60×60

optimal pixel size, e.g., for the CT V.3 system the pixel size is 59 microns, making some binning required. As can be seen from Table 5, the number of useful pixels across the field decreases with the wavelength. This is due to the particular order of the seven system configurations that we have presented here. It is important to note that the AT is limited by astigmatism, and therefore the field aberrations increase with the field angle squared, so going to a shorter wavelength than 0.4 microns will reduce the field of view but also increase the number of useful pixels across the diffraction-limited field. However, even for our shortest wavelength of 0.4 microns, the required pixel size in track 1 is only 0.5 microns, which is nearly equal to the wavelength of light, and this currently presents a technological challenge. On the other hand, the central telescope is limited by aberration coma, as can be seen from the spot diagrams in Figs. 12–14, and as a result, the spot size increases linearly with the field angle, so changing the wavelength for any given variant of the system will not increase the number of useful pixels.

Despite some limitations mentioned above, the proposed system offers a cost-effective solution for future giant telescopes. The multifocal telescope forms several coherent images of the same astronomical object, which can be used simultaneously for various science instruments. The presented results for ray-tracing in a 100-m multifocal telescope can be used for linear scaling of the system to achieve a desired size when operating at a chosen wavelength (Table 5).

Acknowledgments

The authors declare no conflicts of interest.

References

1. R. Tamai et al., "The ESO's ELT construction progress," *Proc. SPIE* **11445**, 114451E (2020).
2. G. Sanders, "The thirty meter telescope (TMT): an international observatory," *J. Astrophys. Astron.* **34**, 81–86 (2013).
3. T. Andersen et al., "The Euro50 extremely large telescope," *Proc. SPIE* **4840**, 214–225 (2003).
4. E. T. Brunetto et al., "Progress of ESO's 100-m OWL optical telescope design," *Proc. SPIE* **5382**, 159–168 (2004).
5. P. A. Lightsey, "James Webb Space Telescope: a large deployable cryogenic telescope in space," *Proc. SPIE* **6720**, 67200E (2007).
6. W. Wild et al., "Millimetron—a large Russian-European submillimeter space observatory," *Exp. Astron.* **23**, 221–244 (2009).

7. D. Leisawitz et al., "Origins Space Telescope: trades and decisions leading to the baseline mission concept," *J. Astron. Telesc. Instrum. Syst.* **7**(1), 011014 (2021).
8. J. A. Corsetti et al., "Optical design of the Origins Space Telescope," *J. Astron. Telesc. Instrum. Syst.* **7**(1), 011010 (2021).
9. D. Puryaev, "Mirror telescopic system," Patent SU1527607A1, USSR J. Invent. 45 (1989).
10. D. Puryaev, "Afocal two-mirror system," *Opt. Eng.* **32**(6), 1325–1327 (1993).

Vladislav V. Druzhin is an assistant professor at the Bauman Moscow State Technical University (BMSTU) of Laser and Optoelectronic Systems Department (RL-2). He received his MS degree in optical from the BMSTU in 2003, and his PhD in optics from the BMSTU in 2008 under the supervision of prof. D.T. Puryaev. His current research interests include astronomical optics, optical metrology, augmented reality (AR), interferometry and holography, optical engineering, and applied optics.

Daniil T. Puryaev received his DSc degree (Eng) from Bauman Moscow State Technical University (BMSTU) in 1958. He is former professor and head of the Laser and Optoelectronic Systems Department (RL-3) of Bauman Moscow State Technical University (BMSTU); the supervisor of 20 PhDs; and the author of more than 300 scientific publications, 100 patents, and four monographs in the fields of optical measurements, aspherical surfaces control, and design of astronomical devices.

Alexander V. Goncharov has been a lecturer in physics at NUI Galway since 2008. From 2003–2008, he was a post-doctoral researcher at the applied optics group, Department of Experimental Physics, NUI Galway, Ireland. He received his PhD from the Department of Astronomy, Lund University, Sweden, with the thesis "Extremely Large Telescopes: Optical Design and Wavefront Correction" in 2003. He received his MSc degree in optical engineering from Moscow Bauman State Technical University, Department of Radio-electronics and Laser Techniques, in 1998.